Published in final edited form as:
Optom Vis Sci. 2012 May ; 89(5): E652–E666. doi:10.1097/OPX.0b013e318238c34e.

Agreement between Retinal Nerve Fiber Layer Measures from Spectralis and Cirrus Spectral Domain OCT

Nimesh B. Patel, OD, FAAO, **Joe L. Wheat, OD**, **Aldon Rodriguez, BS**, **Victoria Tran, BS**, and **Ronald S. Harwerth, OD, PhD, FAAO**
University of Houston, College of Optometry, Houston, Texas (NBP, JLW, RSH), University of California, Berkeley College of Optometry, Berkeley, California (AR), and Southern California College of Optometry, Fullerton, California (VT)

Abstract

Purpose—An assessment of the retinal nerve fiber layer (RNFL) provides important information on the health of the optic nerve. There are several non-invasive technologies, including spectral domain optical coherence tomography (SD-OCT), that can be used for *in vivo* imaging and quantification of the RNFL, but often there is disagreement in RNFL thickness between clinical instruments. The purpose of this study was to investigate the influence of scan centration, ocular magnification and segmentation on the degree of agreement of RNFL thickness measures by two SD-OCT instruments.

Methods—RNFL scans were acquired from forty-five normal eyes using two commercially available SD-OCT systems. Agreement between RNFL thickness measures was determined using each instrument's algorithm for segmentation and a custom algorithm for segmentation. The custom algorithm included ocular biometry measures to compute the transverse scaling for each eye. Major retinal vessels were identified and removed from RNFL measures in 1:1 scaled images. Transverse scaling was also used to compute the RNFL area for each scan.

Results—Instrument derived global RNFL thickness measured from the two instruments correlated well (R^2 = 0.70, p<0.01), but with significant differences between instruments (mean of 6.7 μm; 95% limits of agreement of 16.0 μm to −2.5 μm, ICC = 0.62). For recentered scans with custom RNFL segmentation, the mean difference was reduced to 0.1 μm (95% limits of agreement 6.1 μm to −5.8 μm, ICC = 0.92). Global RNFL thickness was related to axial length (R^2 = 0.24, p<0.01), while global RNFL area measures were not (R^2 = 0.004, p = 0.66). Major retinal vasculature accounted for 11.3±1.6% (Cirrus) or 11.8±1.4% (Spectralis) of the RNFL thickness/area measures.

Conclusions—Sources of disagreement in RNFL measures between SD-OCT instruments can be attributed to the location of the scan path and differences in their retinal layer segmentation algorithms. In normal eyes, the major retinal vasculature accounts for a significant percentage of the RNFL and is similar between instruments. With incorporation of an individual's ocular biometry, RNFL area measures are independent of axial length, with either instrument.

Correspondence to: Nimesh B. Patel.

Corresponding author: Nimesh Patel, University of Houston, College of Optometry, 4901 Calhoun Rd, Houston, Texas 77204, fax: (713) 743-2053, nbpatel2@uh.edu.

Keywords

retinal nerve fiber layer; spectral domain optical coherence tomography; ocular biometry

During the past two decades, there have been important advances in technology for non-invasive imaging of the eye. These technologies have become standard in the diagnosis and management of ocular pathologies, especially those of the posterior segment. In 1991, with the advent of optical coherence tomography, it became possible to image retinal layers with about 8 μm resolution.[1] More recent advances, spectral domain optical coherence tomography (SD-OCT), have increased image capture speed and resolution (down to 4 μm).[2–6]

SD-OCT technology is an important tool for assessing optic neuropathies.[7–13] Specifically, measures of the retinal nerve fiber layer (RNFL), using a standard circular scan 12 degrees in diameter centered on the optic nerve, have considerable diagnostic value. The analysis of the RNFL thickness is based on a quantification of number of pixels of each A-scan image and a pixel-to-micron calculation across each A-scan in the scan path. Thickness measures from each A-scan are often plotted following a path from temporal, superior, nasal, inferior and back to temporal, and commonly referred to as a TSNIT plot. These measures are further quantified as average thickness measures for the entire B-scan, TSNIT plot and/or sector based averages. However, several factors including scan quality, scan centration and the specific segmentation algorithm are known to influence thickness measures derived from SD-OCT images.[14–16] In general, for each instrument, the *in-vivo* RNFL thickness measures are reliable with good repeatability in both normal and diseased eyes.[17–21] In addition, significant changes in RNFL thickness can be detected when the TSNIT average changes by 4–8 μm, dependent on the specific technology and instrument used.[20, 22, 23]

With increasing clinical utility, several commercially available SD-OCT instruments have become available. In theory, the thickness measures quantified from well centered scans of similar dimensions should be identical across instruments. However, both total retinal thickness measures and RNFL thickness measures are significantly different between instruments and cannot be used interchangably.[24–26] To efficiently monitor patients, it is essential that thickness data from current and future instruments be compatible and comparable, especially in monitoring chronic conditions such as glaucoma.

Across SD-OCT instruments, there are two strategies for acquiring B-scans for RNFL analysis. The more common methodology involves sampling from a circular scan path centered on the optic nerve. Alternatively, with scan speeds achieved by most SD-OCT technology, volumetric data, centered on the optic nerve head, can be acquired and circular scan data interpolated to produce OCT B-scans that correspond to a 12 degree diameter circular scan path.[16, 27–29] The two methodologies produce TSNIT measures and either can be used with real-time or offline image registration for signal averaging to improve signal-to-noise ratios for improved retinal layer segmentation. For example, while the Cirrus HD-OCT (Carl Zeiss Meditec Inc, Dublin, CA) interpolates scans from volumetric data centered on the optic nerve, the Spectralis SD-OCT (Heidelberg Engineering, Heidelberg, Germany) uses a circular scan path to capture RNFL B-scans. Although RNFL thickness measures from both these instruments are correlated, significant differences have been reported for global and quadrant thicknesses.[21, 26] The most notable difference comparing these two techniques has been in the nasal quadrant for which the agreement has a significant linear relationship (slope = 0.7, intercept = −42.13 μm).[21]

In addition to the technology of image acquisition, other factors such as axial length, size and shape of the optic nerve head, age, and non-neuronal content, should be considered in evaluating global (average) or quadrant measures of RNFL thickness.[29–33] Specifically, RNFL thickness measures are thinner in eyes that are older, longer and have a smaller optic nerve size. It is well established that thickness changes that occur with age are a reflection of the associated loss of retinal ganglion cells, corresponding to between 0.3 and 0.6% loss/year.[34–38] The relationship of RNFL thickness and axial length has been attributed to ocular magnification, and the location of the scan path and, after compensation for ocular magnification, cross sectional area measures of the RNFL are not related to axial length.[29, 31, 39, 40] Both histological and in-vivo studies in human and non-primates suggest a relationship between optic nerve head size and total axonal content within the optic nerve.[41–43] The RNFL also has significant non-neuronal components, including glial and vascular tissue (Mardin, CY, et al. IOVS 2009;50,ARVO E-abstract 3333).[44, 45] In addition, with glaucomatous disease progression, an increase in glial tissue and decrease in vascular components have been noted (Wheat, JL, et al. IOVS 2009;50,ARVO E-abstract 5826).[46–48] Thus, there are many biometric and biological factors that need to be included in assessing OCT measurements of RNFL thickness, especially for management of clinical patients.

As OCT technology evolves, for RNFL measures to be used as a diagnostic tool in optic neuropathy diagnosis and management, it is essential that measures can be compared across instruments. This is especially true for chronic conditions such as glaucoma where both neuronal and non-neuronal changes take place over several years. The present investigation was undertaken to address these discrepancies by comparing RNFL thickness measures acquired using two SD-OCT instruments that use different methodologies to capture the 12 degree circular TSNIT scan. The influence of segmentation, ocular biometry and the major retinal vessel content to RNFL thickness measures using both technologies was investigated. Some of the results of these studies have been presented briefly elsewhere (Patel, NB, et al. IOVS 2011;52,ARVO E-abstract 173).

METHODS AND MATERIALS

Subjects

Fifty healthy subjects, 21–68 yrs of age, with no prior history of ocular pathology were recruited for this study. All subjects were patients, students or staff at the University of Houston, University Eye Institute. The study adhered to the tenets of the Declaration of Helsinki, and all aspects of the study were reviewed by the committee for protection of human subjects at the University of Houston. Informed consent was obtained from all subjects.

Prior to enrollment, subjects were screened using visual acuity, standard automated perimetry 24–2 visual fields, intraocular pressure measures, slit lamp examination and dilated fundus evaluation to ensure good ocular health. One randomly selected eye from each subject was used for data analysis. Of these, five eyes that had either undocumented pathology or excessive eye movements during SD-OCT scanning were excluded from data analysis.

Optical Coherence Tomography

SD-OCT scans were acquired from subjects at least 30 minutes after pupils were dilated with 1% tropicamide and 2.5% phenylephrine. Three scan patterns/protocols were used to acquire high resolution scans using the Spectralis HRA+OCT (Heidelberg Engineering, Heidelberg, Germany, Software version 5.1.3) that included; 1) 12 radial scans centered on the optic nerve head, 2) a 12 degree circular scan centered on the optic nerve head, and 3) a

49 line raster scan, 20×20 centered on the fovea. For noise reduction, B-scan averaging was set at 16 frames for all scan protocols. Scans were repeated if image overlap was noted as frames were being averaged or if the scan had excessive noise, determined as an image quality of < 20 dB. A maximum of three attempts were made to obtain good scans when needed. The unaltered scan data were exported in raw (.vol) files, for analysis using custom MATLAB (The Mathworks, Inc., Natwick, MA) programs.

Two scan protocols using the Cirrus HD-OCT (Carl Zeiss Meditec Inc, Dublin, CA, Software version 5.0.0) scans were acquired on all subjects; 1) the high resolution macular cube scan centered on the fovea, and 2) 200×200 A-scans centered on the optic nerve. Scans were repeated if motion was detectable on the *en face* reflectance image or when the scan quality was < 8/10. A maximum of three attempts were made to obtain good scans when needed. The scan data were exported as raw (.dat, .bin, .img, .txt) files using the Carl Zeiss Meditec Research Browser (version 5.0.0.326).

Ocular Biometry and Scaling

Axial lengths, corneal curvatures, and anterior chamber depths were measured using the IOL Master (Carl Zeiss Meditec, Inc., Dublin, CA). Transverse scaling for each eye was computed using a three surface schematic eye, using methods described by Bennett and Rabbetts.[49–51] Lens parameters including lens thickness and curvature were interpolated from normative data.[52] Refractive indices of the ocular components were determined using a wavelength of 855 nm, corresponding to the mean of the central wavelengths for the Cirrus (840 nm) and Spectralis (870 nm) OCT sources.[53, 54] The constructed schematic eyes were used to compute the transverse scaling at the retina assuming a spherical retina as previously described.[29] Transverse scaling was used to compute the circumference of the scan path, which was then used to compute the RNFL estimated integral or area.[29, 40]

Instrument Algorithm Based RNFL Analysis

The raw data exports from the Cirrus and Spectralis SD-OCT RNFL scans were used to determine the global, quadrant and sector thickness data. The first 30 degree sector was centered on the temporal quadrant and subsequent sectors were numbered in a clockwise manner referenced to the left eye (Fig 4C). Along with Bland-Altman plots, intraclass correlation coefficient (ICC) and paired t-tests were used to assess agreement between thickness measures from the two instruments. The influence of scan centration was investigated using the raw export data from the Cirrus HD-OCT that contained RNFL segmentation data for the entire 200×200 A-scan region. To investigate the influence of scan alignment using Cirrus HD-OCT data, custom MATLAB programs were used to interpolate RNFL thickness profiles for scans displaced up to 500 μm from the center of the nerve. The mean change, in global RNFL thickness from these interpolations, for all subjects in this study is illustrated in figure 1, and follows systematic trends previously noted.[15, 16, 55]

To evaluate the influence of scan path differences on sector and global thickness differences, RNFL scans with identical locations were compared. This was achieved by aligning the two scans, and interpolating RNFL scans from the RNFL thickness map from the Cirrus data that were identical to that of the Spectralis RNFL scan path. The Cirrus fundus image used for registration was constructed from the volume data where the pixel intensity for each A-scan from the 200×200 scanned region was averaged to create a 2D image (Fig 2B). This reflectance image was registered to the infrared scanning laser ophthalmoscope (SLO) image from the Spectralis scan using a generalized dual bootstrap iterative closest point algorithm (i2k retina, DualAlign LLC, Clifton, NY).[56] The scan path, extracted from the Spectralis raw data export, was mirrored on the Cirrus reflectance image and used to determine the RNFL thickness as quantified by the instrument's algorithm (Fig 2E). In

addition, the aligned images were used to determine the differences in ocular magnification, which was calculated as the square root of pixel content ratio between the two fundus images, assuming a scan angle of 30 degree for the Spectralis and 20 degrees for the Cirrus (Eq 1).

$$\text{Difference in Ocular Magnification} = \frac{\sqrt{\text{Number of Pixels Spectralis SLO}}}{\sqrt{\text{Number of Pixels Cirrus Reflectance Image}}} \times \frac{20}{30}$$

Custom RNFL Torsional Alignment

All SD-OCT instruments have chin and forehead rests, which allow horizontal and vertical eye alignment, but not torsional alignment. Previous studies have shown that significant cyclotorsional eye movements occur during fixation, especially with reduced visual stimuli as occurs during OCT imaging.[57, 58] Torsional eye movements can influence quadrant and sector RNFL thickness measures and identification of thinning, especially with respect to the normative TSNIT plot. Although the Spectralis software aligns RNFL scans to the macula, it is highly dependent on; 1) accurate centration of the scan and, 2) accurate fixation by the patient when scan aquisition and averaging is started. Hence, alignment using anatomical landmarks may provide for better accuracy and repeatability.

Torsional eye position was compensated for by aligning the center of the optic nerve to the foveal pit for each subject. The center of the fovea was identified as the thinnest region within the raster scan of the macular region. This center was refined by fitting the thickness profile of the pit region with best fit circles from 30–75% of the pit height and using the geometric mean of these as the refined pit center (Patel, NB, et al. IOVS 2009;50,ARVO E-abstract 6207). The neural canal opening (NCO) was manually identified using radial scans through the optic nerve. The NCO was fit with an ellipse, which was used to determine the center of the optic nerve.[29, 59] The SLO images for the scans centered on the optic nerve and on the macula were registered using the i2k Retina software. All RNFL scans were subsequently referenced to the line fit between the centers of the fovea and optic nerve as illustrated in figure 3.

Custom RNFL Segmentation

The standard Cirrus 12 degree circular scan used for RNFL thickness analysis consist of 512 A-scans interpolated from a 200×200 A-scan volume, spanning a nominal region of 20×20 degrees. In contrast, the Spectralis, high resolution 12 degree circular scan, consists of 1536 A-scans acquired in a circular path. In addition, the scan depth of the Cirrus is up to 2 mm, whereas the maximum depth for Spectralis images is 1.92 mm. To match the scans, using the image registered data, the Cirrus volume scans were interpolated to obtain 1536 A-scans and cropped to a maximum height measuring 1.92 mm, to match the same locations obtained for Spectralis circular scans.

A custom MATLAB program identified the inner limiting membrane and junction between the RNFL and ganglion cell layer. To enhance layer visibility, images were first de-noised using an haar two dimensional stationary wavelet, and convolved with a Gaussian filter with a standard deviation of 4. Signal intensity profiles for each A-scan were then used to identify the RNFL, as previously described.[29] Errors in segmentation, that were most common around retinal vessels, were corrected manually. To reduce bias, a total of 4 RNFL scans from the Cirrus, with different scan centers, were segmented and analyzed by the user who was unaware of which scan was from the registered scan path.

The RNFL B-scan from the Spectralis is an averaged image for up to 16 B-scans. The time taken to capture these scans often spans several diastolic and systolic phases. If retinal vessels change significantly in size during these phases, the non-neuronal retinal vessel content within the RNFL would be different between averaged and non-averaged scans. To account for the retinal vasculature, B-scans were first scaled to a 1:1 aspect ratio using the computed transverse scaling from the 3 surface schematic eye. The borders of the shadows cast by the retinal vasculature were identified and marked. The center of each vessel within the retinal tissue was then manually identified. The thickness of the RNFL within the circular region marked by the vessel center and shadow borders was subtracted from the total thickness and determined as the RNFL vascular contribution (Fig. 4). The RNFL area for each A-scan was computed as the RNFL thickness multiplied by its width. The average RNFL thickness and sum of RNFL areas, with and without retinal vasculature, for the 1536 A-scans were used for data analysis.

RESULTS

RNFL Thickness - Instrument Algorithm

For the 45 eyes included in the data analysis, the average image quality for RNFL scans was 30.6 ± 4.93 and 9.0 ± 0.82 for the Spectralis and Cirrus scans, respectively. The average RNFL global thickness measurement was 97.9 ± 7.9 μm for the Spectralis and 91.2 ± 8.4 μm for the Cirrus. The agreement of RNFL measures using each of the two instruments was assessed using Bland-Altman plots, the intraclass correlation coefficient (ICC) and paired t-tests. Bland-Altman plots provide a graphical method for comparing the two methodologies. The mean difference, and 95% limits of agreement can be used to assess if the difference between two methodologies are clinically acceptable.[60] The intraclass correlation coefficient (ICC) is a measure of reliability, calculated by comparing the between-subject variances to overall variance. In general, agreement is considered good, when the within subject variance is a third of the between-subject variance (ICC ≥ 0.75) represent good agreement between measures.[61] Paired t-tests were also used to test the hypothesis that the difference in RNFL thickness measures from the two instruments is zero.

Based on these statistics, there was overall poor agreement of RNFL thickness between the two instruments, with the least agreement for the nasal quadrant (Table 1). Similarly, Bland-Altman plots (Fig. 5) indicate significant thickness differences in all quadrants, along with a systematic discrepancy for nasal quadrant thicknesses (slope = 0.51, intercept = −27.19, R^2 = 0.34, $p < 0.01$). In addition, the standard deviation of thickness differences for each quadrant, except for the temporal quadrant was at least half the standard deviation for thickness measured from each instrument.

Scan Alignment

Various methods are used to center the RNFL scan on the optic nerve. For example, the Spectralis relies on the user to visually center the scan on the optic nerve. A circular guide, the size of an average optic nerve, is projected on the real time SLO image to aid in centering. In addition, when an internal nasal fixation target is used, the scan is referenced to the center of the optic nerve and fixation. Alternatively, the Cirrus obtains a 200×200 volume scan of the optic nerve and an automated process is used to determine the geometric center of the optic nerve head after the rim margin has been identified. The RNFL scan is interpolated from the volumetric data at a fixed distance from the center of the optic nerve head. These volumetric data can also be used to investigate the effect of scan alignment, which for the eyes included in this study, resulted in an average maximum change in thickness of 14.8 ± 5.3 μm (Fig. 1) for misalignments of the scan by up to 500 μm.

The SLO fundus image from the Spectralis and reflectance fundus image from the Cirrus were successfully registered for all the subjects using a generalized dual bootstrap iterative closest point image registration algorithm.[56] The difference in scan center location between the two instruments, using the registered images, was 117.7 ± 70.2 μm. Realignment of the Cirrus scan to match that of the Spectralis had a minimal effect on the thickness differences (Table 2). In addition, using the modeled average thickness data from varying scan alignment (Fig. 1), the differences in scan location measured, was predicted to account for only 0.45 ± 0.4 μm of the thickness differences.

Along with horizontal and vertical misalignments, torsional differences between the fundus images from the two instruments were also evident. The TSNIT thickness plots were shifted according to the average angular difference between the two images. To realize the greatest match, the plots were also shifted to the point with the highest cross correlation. The average rotational difference, using these methods, was 6.4 ± 3.8 degrees. Realignment using all three dimensions improved the ICC for each quadrant (Table 2).

Custom Segmentation and Retinal Vascular Contribution

The custom segmentation program consistently measured a larger RNFL thickness for both Spectralis (11.4 ± 3.7 μm) and Cirrus (18.8 ± 3.5 μm) scans, compared to the instrument algorithms. In addition, these custom measures were significantly different ($p < 0.01$) for most quadrants and sectors for both instruments. However, the agreement for RNFL thickness measures, as determined by ICC and paired t-test, comparing custom segmentation to the instrument algorithm, was better for Spectralis scans (Table 3). Overall, the agreement between instruments improved with custom segmentation. For the Bland-Altman plot, the standard deviation were; 1) less than with the instrument algorithm, 2) less than half the standard deviation for the range of thicknesses for each measure. Good agreement for RNFL measures were also indicated by ICC and t-test statistics. For global RNFL thickness, the mean difference was 0.1±3.1 μm, ICC = 0.92, $p = 0.59$ (Table 5).

The major retinal vasculature accounted for ~11% (11.8±1.5% Cirrus, 11.3±1.6% Spectralis) of the global RNFL thickness (Table 4). Superior and inferior quadrants had the greatest major retinal vascular contribution with the temporal quadrant having the least (Table 4). Differences for major retinal vascular contribution was insignificant for the segmentations from the two instruments ($p > 0.05$, $\beta < 0.18$ for all quadrants). Although there was very good agreement in vascular contribution, the vascular location in the registered B-scans were not always identical. In addition, some small vessels were clearly visible in one B-scan, but not the other, as illustrated in figure 7.

Ocular Biometry and RNFL Area

For the healthy eyes included in this study, axial lengths ranged from 22.3 mm to 27.9 mm, and were normally distributed with a mean of 24.7 ± 1.32 mm. The global RNFL thickness, as determined by the instrument algorithm, decreased with increase in axial length, with a slope of −3.1 μm/mm for the Spectralis ($p < 0.01$), and −3.1 μm/mm for the Cirrus ($p < 0.01$) (Fig. 8). Although thickness measures between instruments were significantly different, the slope of the function was not ($p = 0.95$). Similarly, for the custom segmentation data, the slope of RNFL thickness vs. axial length was −3.0 μm/mm ($p < 0.01$, $R^2 = 0.24$, Fig 8B).

A significant relationship between axial length and ocular magnification ratio, as determined using the registered fundus images, would indicate differences in the optics of the two imaging devices ($R^2 = 0.41$, $p < 0.01$, Fig 8C). For the majority of the scans, the region of the retina scanned per degree of scan angle was smaller for Spectralis images, and was similar for only significantly longer eyes. However, this difference did not alter the location

of the scan paths significantly, as illustrated by the similarity in RNFL thickness at all axial lengths using the custom segmentation (Fig 8B).

The thinner RNFL measures for longer axial lengths should not reflect on a difference in retinal ganglion cell axonal content, but rather illustrates changes in RNFL thickness and density associated with distance from the optic nerve rim margin.[42, 62, 63] However, the cross sectional area of the RNFL should be independent of scan distance from the optic nerve head rim margin within the peripapillary region were a low density of ganglion cells are present.[64] RNFL area measures were computed by multiplying the scan circumference, as determined using the computed transverse scaling, and the global RNFL thickness.[29, 40] The RNFL area was not related to axial length (Spectralis: $p = 0.69$, Cirrus: $p = 0.66$) and was similar for the two instrument (Fig 8D).

DISCUSSION

High resolution imaging of retinal structure has become standard in clinical care and several technologies, including scanning laser polarimetry, confocal scanning laser ophthalmoscopy, and optical coherence tomography (OCT) are available to image and measure structures of the posterior segment of the eye. However, only OCT provides cross section images of the retina to visualize and quantify the individual retinal layers. Recent advances in this technology, spectral domain optical coherence tomography (SD-OCT), enable imaging of the eye at high speeds with axial resolutions down to 5 μm.

Although there are several clinical SD-OCT instruments which all use similar technology and capture comparable images, clinical studies have shown that the thickness measures of retinal structures are significantly different between instruments.[21, 26, 28, 65] In studies comparing RNFL thickness measures from the Spectralis SD-OCT and Cirrus HD-OCT, although measures from both instruments were repeatable, a significant difference was reported between instruments.[21] Similar to the present study, a linear relationship was reported for the agreement for the nasal quadrant (slope = 0.70).[21] The principal finding of present investigation is that the underlying sources for the differences in measurements are related to software applications for image segmentation and data analysis procedures, rather than in the data acquisition. Therefore, to detect changes, such as progressive glaucomatous neuropathy, either an identical instrument would need to be used for follow-up, or the raw data would need to be analyzed by algorithms that include ocular biometry and identical image segmentation across instruments.

The present investigation was based on the agreement in retinal nerve fiber layer thickness between two specific SD-OCT instruments, i.e., the Cirrus HD-OCT (Carl Zeiss Meditec Inc, Dublin, CA), and Spectralis HRA+OCT (Heidelberg Engineering, Heidelberg, Germany). The selection of the two SD-OCT systems was rooted in the different scanning protocols used to acquire the standard circular B-scan used for RNFL quantification. While the Spectralis uses a circular scan path, which the user centers on the optic nerve, the Cirrus interpolates the scan from a 200×200 A-scan cube centered on the optic nerve. In addition, the Spectralis allows for real time eye tracking and averaging of B-scans to increase the signal to noise ratio. Thus, while the specific results apply to these clinical instruments, the overall results should be generalized to other SD-OCT instruments.

In agreement with previous studies[21, 26, 65, 66] it was shown that for eyes with no history of optic neuropathy, there were significant differences in the RNFL thickness measures between the Spectralis and Cirrus SD-OCT systems, using the instrument-based analysis. The 95 % agreement for global thickness was better than that for average quadrant thickness measurements using the instrument image analysis algorithm (Fig 5). However, the limits of

agreement for global thickness measures (−2.5–16.0 μm) had a range half that of the total range of thickness measures for either instrument (37.8 μm Cirrus, 33.3 μm Spectralis). In addition, the difference in thickness measures for the nasal quadrant was related to the average thickness measures of the two instruments. However, the mean difference in thickness measures for the global and quadrant thickness was different from previously reported results[26, 65, 66]. The differences could be a reflection on differences in subjects or in the instrument software versions. Whereas previous studies have investigated normal and glaucoma subjects, only healthy eyes were included in the present study. In addition, both instruments have undergone several software upgrades from the previous studies. However, the more important sources of discrepancy in thickness measures were scan alignment, ocular magnification, and segmentation. The influence of scan alignment and centration has been investigated using both time domain and spectral domain OCT systems.[16, 28, 55] The general finding of these studies is that a misalignment of the scan, in either the horizontal and vertical direction has a significant impact on both the shape of the TSNIT thickness plots and global RNFL thickness measures. A similar pattern, with up to 14 μm of global RNFL thickness change, was noted when the center of the RNFL scan was displaced for the Cirrus data (Fig. 1). However, centering the Cirrus scan to match that of the Spectralis, had only a small increase in agreement of global RNFL thickness (Table 2).

The relatively small improvement in agreement between instruments with only adjustment for scan centration can be explained by differences in torsional eye position during scanning movements of the eyes. Specifically, although a head tilt does not change global thickness, it has a significant effect on the shape of the TSNIT plot.[67] This redistribution of thickness along the TSNIT plot results in significant differences in both sector and quadrant thicknesses and associated changes in the thickness distribution with respect to normative data. By taking into account torsional eye alignment differences, and their influence on the scan path, there were substantial improvements in the agreement of quadrant thickness measures for the two instruments (Table 2), although, the thickness measures from the two instruments were still significantly different. Although referencing RNFL scans to the center of the optic nerve and the internal fixation target, as is done with Spectralis RNFL scans, improves alignment, detection of these landmarks using anatomical features may be useful in individuals with poor fixation.

It is logical that although there can be slight differences in the characteristics of the various OCT instruments, the images from these systems should be similar, with comparable RNFL thickness.[68, 69] This result was demonstrated by the significant improvement in instrument agreement for RNFL thicknesses with B-scans that were registered, aligned to the fovea, and analyzed by the same segmentation protocol (Fig 6, Table 5). The Bland-Altman plots illustrated a smaller standard deviation for all quadrants, compared to instrument analysis. The largest standard deviation was in the nasal quadrant, which also had the greatest improvement in thickness agreement, and had the largest number of segmentation errors requiring manual correction. The failure of the program to accurately segment this region is probably due to the reduced signal in the nasal quadrant that is attributable to the characteristics of the optical scan angle.[70] Overall, the custom segmentation results in larger RNFL thickness measures compared to either instrument algorithm. This increased thickness can be attributed to the method by which the algorithm dealt with retinal vasculature. Whereas most instrument algorithm tend to 'skip' across retinal vessels, the custom algorithm outlines each vessel that contributes to the RNFL, and has no smoothing artifact (Fig. 4&7). Hence, agreement between custom and instrument segmentation was greatest for the temporal quadrant which also had the smallest contribution from major retinal vasculature.

For an accurate assessment of the axonal content within the RNFL, the non-neuronal content within the layers should be excluded. Although glial tissue cannot be visualized using current technology, the major retinal vasculature cast shadows within the B-scan, and can be accounted for (Mardin, CY, et al. IOVS 2009;50,ARVO E-abstract 3333).[45] After the SD-OCT scans had been rescaled to a 1:1 aspect ratio, the custom algorithm allowed the user to manually select the center of each vessel identified, and subtract the vessel area from the scan image.[29] Using this technique, major retinal vasculature contribution to RNFL thickness in healthy eyes was ~11%, and similar for the two instruments (Table 2). These measures were in agreement with those reported by Mardin, et al. (11%), but are slightly less than reported by Hood et al. (13%).[45] The vascular contribution is actually larger than that reported in this study, because there were instances where vessels were noted in the B-scan of one instrument but not in the other (Fig 7), and small vessels and capillaries cannot be visualized and excluded.[71, 72]

An additional factor that is necessary to consider when analyzing the RNFL thickness is ocular biometry. Specifically, the thickness of the RNFL measured using the traditional 12 degree circular scan is a function of axial length.[29, 30, 63] This relationship with axial length was similar for both instrument- and custom-segmentation for both systems (Fig 8), which is a direct reflection of the projection of the scan path in relationship to the optic nerve rim margin for different sized eyes. Although the RNFL thickness decreases as the scan path increases in distance from the rim margin, the thickness change is related to retinal ganglion cell axon density rather than the number of axons within the region.[29, 63, 64] It is then logical that the area of the RNFL within the scanned region, which reflects the axonal content, is poorly correlated with axial length (Fig 8). Similarly, an alternative method to compensate for thickness changes with scan distance from the nerve is to rescale RNFL thickness measures using axial length as illustrated by Kang, et al.[31]

Both RNFL area and rescaling of RNFL thickness computations require consideration of the optics of the eye and instrument being used.[50, 51, 73, 74] Although biometry of the eye is measured efficiently and accurately using non-contact low coherence reflectometry, the optical properties of scanning laser devices are proprietary, and usually unknown to the clinician or researcher. The influence of instrument optics on ocular magnification can be investigated for the same eye imaged using both instruments with image registration (Fig 2). Using these methods, a significant difference in ocular magnification, related to axial length was noted for the Cirrus and Spectralis SD-OCT systems (Fig 8C). However, these differences were not large enough to cause any appreciable divergence in the scan path, as noted by the similarity in thickness and area measures for varying axial lengths (Fig 8).

In conclusion, the results of these investigations have demonstrated the utility of methods for comparing measurements of retinal morphology across SD-OCT instruments. Specifically, images captured using two different SD-OCT instruments (Cirrus and Spectralis) were shown to be similar when similar image processing methods were used. The apparent differences in RNFL thickness with the embedded instrument algorithms, previously reported in the literature and confirmed by the present study, are explained by differences in scan path and segmentation methodologies. Thus, the results demonstrate the importance of considering both scan centration, and differences in torsional eye position when comparing quadrant thickness measures between instruments. In addition, with application of a common methodology for transverse magnification and segmentation of the retinal layers the RNFL thickness measures, with and without compensation for major retinal vessels, will be comparable between instruments. Finally, by incorporating ocular biometry, the scaled measures of RNFL area are independent of axial length.

Acknowledgments

Research Support: R01 EY001139 (RSH), K23 EY018329 (JW), P30 EY007551, Optometric Glaucoma Society Ezell Fellowship (NBP), John and Rebecca Moores Professorship (RSH).

REFERENCES

1. Huang D, Swanson EA, Lin CP, Schuman JS, Stinson WG, Chang W, Hee MR, Flotte T, Gregory K, Puliafito CA, et al. Optical coherence tomography. Science. 1991; 254:1178–1181. [PubMed: 1957169]
2. Chen TC, Cense B, Pierce MC, Nassif N, Park BH, Yun SH, White BR, Bouma BE, Tearney GJ, de Boer JF. Spectral domain optical coherence tomography: ultra-high speed, ultra-high resolution ophthalmic imaging. Arch Ophthalmol. 2005; 123:1715–1720. [PubMed: 16344444]
3. Nassif N, Cense B, Park B, Pierce M, Yun S, Bouma B, Tearney G, Chen T, de Boer J. In vivo high-resolution video-rate spectral-domain optical coherence tomography of the human retina and optic nerve. Opt Express. 2004; 12:367–376. [PubMed: 19474832]
4. Nassif N, Cense B, Park BH, Yun SH, Chen TC, Bouma BE, Tearney GJ, de Boer JF. In vivo human retinal imaging by ultrahigh-speed spectral domain optical coherence tomography. Opt Lett. 2004; 29:480–482. [PubMed: 15005199]
5. Fujimoto JG. Optical coherence tomography for ultrahigh resolution in vivo imaging. Nat Biotechnol. 2003; 21:1361–1367. [PubMed: 14595364]
6. Sakamoto A, Hangai M, Yoshimura N. Spectral-domain optical coherence tomography with multiple B-scan averaging for enhanced imaging of retinal diseases. Ophthalmology. 2008; 115:1071–1078. [PubMed: 18061270]
7. Wheat JL, Rangaswamy NV, Harwerth RS. Correlating RNFL thickness by OCT with perimetric sensitivity in glaucoma patients. J Glaucoma. 2011 [Epub ahead of print].
8. Costello F, Coupland S, Hodge W, Lorello GR, Koroluk J, Pan YI, Freedman MS, Zackon DH, Kardon RH. Quantifying axonal loss after optic neuritis with optical coherence tomography. Ann Neurol. 2006; 59:963–969. [PubMed: 16718705]
9. Sergott RC. Optical coherence tomography: measuring in-vivo axonal survival and neuroprotection in multiple sclerosis and optic neuritis. Curr Opin Ophthalmol. 2005; 16:346–350. [PubMed: 16264344]
10. Ratchford JN, Quigg ME, Conger A, Frohman T, Frohman E, Balcer LJ, Calabresi PA, Kerr DA. Optical coherence tomography helps differentiate neuromyelitis optica and MS optic neuropathies. Neurology. 2009; 73:302–308. [PubMed: 19636050]
11. Schuman JS, Hee MR, Puliafito CA, Wong C, Pedut-Kloizman T, Lin CP, Hertzmark E, Izatt JA, Swanson EA, Fujimoto JG. Quantification of nerve fiber layer thickness in normal and glaucomatous eyes using optical coherence tomography. Arch Ophthalmol. 1995; 113:586–596. [PubMed: 7748128]
12. Horn FK, Mardin CY, Laemmer R, Baleanu D, Juenemann AM, Kruse FE, Tornow RP. Correlation between local glaucomatous visual field defects and loss of nerve fiber layer thickness measured with polarimetry and spectral domain OCT. Invest Ophthalmol Vis Sci. 2009; 50:1971–1977. [PubMed: 19151389]
13. Townsend KA, Wollstein G, Schuman JS. Imaging of the retinal nerve fibre layer for glaucoma. Br J Ophthalmol. 2009; 93:139–143. [PubMed: 19028735]
14. Sung KR, Wollstein G, Schuman JS, Bilonick RA, Ishikawa H, Townsend KA, Kagemann L, Gabriele ML. Scan quality effect on glaucoma discrimination by glaucoma imaging devices. Br J Ophthalmol. 2009; 93:1580–1584. [PubMed: 19692363]
15. Vizzeri G, Bowd C, Medeiros FA, Weinreb RN, Zangwill LM. Effect of signal strength and improper alignment on the variability of stratus optical coherence tomography retinal nerve fiber layer thickness measurements. Am J Ophthalmol. 2009; 148:249–255. [PubMed: 19427621]
16. Gabriele ML, Ishikawa H, Wollstein G, Bilonick RA, Townsend KA, Kagemann L, Wojtkowski M, Srinivasan VJ, Fujimoto JG, Duker JS, Schuman JS. Optical coherence tomography scan circle location and mean retinal nerve fiber layer measurement variability. Invest Ophthalmol Vis Sci. 2008; 49:2315–2321. [PubMed: 18515577]

17. Langenegger SJ, Funk J, Toteberg-Harms M. Reproducibility of retinal nerve fiber layer thickness measurements using the eye tracker and the retest function of Spectralis SD-OCT in glaucomatous and healthy control eyes. Invest Ophthalmol Vis Sci. 2011; 52:3338–3344. [PubMed: 21330656]
18. Blumenthal EZ, Williams JM, Weinreb RN, Girkin CA, Berry CC, Zangwill LM. Reproducibility of nerve fiber layer thickness measurements by use of optical coherence tomography. Ophthalmology. 2000; 107:2278–2282. [PubMed: 11097610]
19. Carpineto P, Ciancaglini M, Zuppardi E, Falconio G, Doronzo E, Mastropasqua L. Reliability of nerve fiber layer thickness measurements using optical coherence tomography in normal and glaucomatous eyes. Ophthalmology. 2003; 110:190–195. [PubMed: 12511365]
20. Budenz DL, Fredette MJ, Feuer WJ, Anderson DR. Reproducibility of peripapillary retinal nerve fiber thickness measurements with stratus OCT in glaucomatous eyes. Ophthalmology. 2008; 115:661–666. [PubMed: 17706287]
21. Tan BB, Natividad M, Chua KC, Yip LW. Comparison of retinal nerve fiber layer measurement between 2 spectral domain OCT instruments. J Glaucoma. 2011 [Epub ahead of print].
22. Leung CK, Cheung CY, Weinreb RN, Qiu Q, Liu S, Li H, Xu G, Fan N, Huang L, Pang CP, Lam DS. Retinal nerve fiber layer imaging with spectral-domain optical coherence tomography: a variability and diagnostic performance study. Ophthalmology. 2009; 116:1257–1263. [PubMed: 19464061]
23. Mwanza JC, Chang RT, Budenz DL, Durbin MK, Gendy MG, Shi W, Feuer WJ. Reproducibility of peripapillary retinal nerve fiber layer thickness and optic nerve head parameters measured with cirrus HD-OCT in glaucomatous eyes. Invest Ophthalmol Vis Sci. 2010; 51:5724–5730. [PubMed: 20574014]
24. Bengtsson B, Andersson S, Heijl A. Performance of time-domain and spectral-domain Optical Coherence Tomography for glaucoma screening. Acta Ophthalmol. 2010 [Epub ahead of print].
25. Giani A, Cigada M, Choudhry N, Deiro AP, Oldani M, Pellegrini M, Invernizzi A, Duca P, Miller JW, Staurenghi G. Reproducibility of retinal thickness measurements on normal and pathologic eyes by different optical coherence tomography instruments. Am J Ophthalmol. 2010; 150:815–824. [PubMed: 20965494]
26. Leite MT, Rao HL, Weinreb RN, Zangwill LM, Bowd C, Sample PA, Tafreshi A, Medeiros FA. Agreement among spectral-domain optical coherence tomography instruments for assessing retinal nerve fiber layer thickness. Am J Ophthalmol. 2011; 151:85–92. e1. [PubMed: 20970108]
27. Kim JS, Ishikawa H, Sung KR, Xu J, Wollstein G, Bilonick RA, Gabriele ML, Kagemann L, Duker JS, Fujimoto JG, Schuman JS. Retinal nerve fibre layer thickness measurement reproducibility improved with spectral domain optical coherence tomography. Br J Ophthalmol. 2009; 93:1057–1063. [PubMed: 19429591]
28. Kim JS, Ishikawa H, Gabriele ML, Wollstein G, Bilonick RA, Kagemann L, Fujimoto JG, Schuman JS. Retinal nerve fiber layer thickness measurement comparability between time domain optical coherence tomography (OCT) and spectral domain OCT. Invest Ophthalmol Vis Sci. 2010; 51:896–902. [PubMed: 19737886]
29. Patel NB, Luo X, Wheat JL, Harwerth RS. Retinal nerve fiber layer assessment: area versus thickness measurements from elliptical scans centered on the optic nerve. Invest Ophthalmol Vis Sci. 2011; 52:2477–2489. [PubMed: 21220552]
30. Budenz DL, Anderson DR, Varma R, Schuman J, Cantor L, Savell J, Greenfield DS, Patella VM, Quigley HA, Tielsch J. Determinants of normal retinal nerve fiber layer thickness measured by Stratus OCT. Ophthalmology. 2007; 114:1046–1052. [PubMed: 17210181]
31. Kang SH, Hong SW, Im SK, Lee SH, Ahn MD. Effect of myopia on the thickness of the retinal nerve fiber layer measured by Cirrus HD optical coherence tomography. Invest Ophthalmol Vis Sci. 2010; 51:4075–4083. [PubMed: 20237247]
32. Huynh SC, Wang XY, Rochtchina E, Mitchell P. Peripapillary retinal nerve fiber layer thickness in a population of 6-year-old children: findings by optical coherence tomography. Ophthalmology. 2006; 113:1583–1592. [PubMed: 16949443]
33. Bendschneider D, Tornow RP, Horn FK, Laemmer R, Roessler CW, Juenemann AG, Kruse FE, Mardin CY. Retinal nerve fiber layer thickness in normals measured by spectral domain OCT. J Glaucoma. 2010; 19:475–482. [PubMed: 20051888]

34. Harwerth RS, Wheat JL, Rangaswamy NV. Age-related losses of retinal ganglion cells and axons. Invest Ophthalmol Vis Sci. 2008; 49:4437–4443. [PubMed: 18539947]
35. Harman A, Abrahams B, Moore S, Hoskins R. Neuronal density in the human retinal ganglion cell layer from 16–77 years. Anat Rec. 2000; 260:124–131. [PubMed: 10993949]
36. Balazsi AG, Rootman J, Drance SM, Schulzer M, Douglas GR. The effect of age on the nerve fiber population of the human optic nerve. Am J Ophthalmol. 1984; 97:760–706. [PubMed: 6731540]
37. Da, Pozzo S.; Iacono, P.; Marchesan, R.; Minutola, D.; Ravalico, G. The effect of ageing on retinal nerve fibre layer thickness: an evaluation by scanning laser polarimetry with variable corneal compensation. Acta Ophthalmol Scand. 2006; 84:375–379. [PubMed: 16704701]
38. Repka MX, Quigley HA. The effect of age on normal human optic nerve fiber number and diameter. Ophthalmology. 1989; 96:26–32. [PubMed: 2919049]
39. Savini G, Barboni P, Parisi V, Carbonelli M. The influence of axial length on retinal nerve fibre layer thickness and optic-disc size measurements by spectral-domain OCT. Br J Ophthalmol. 2011 [Epub ahead of print].
40. Bayraktar S, Bayraktar Z, Yilmaz OF. Influence of scan radius correction for ocular magnification and relationship between scan radius with retinal nerve fiber layer thickness measured by optical coherence tomography. J Glaucoma. 2001; 10:163–169. [PubMed: 11442177]
41. Jonas JB, Schmidt AM, Muller-Bergh JA, Schlotzer-Schrehardt UM, Naumann GO. Human optic nerve fiber count and optic disc size. Invest Ophthalmol Vis Sci. 1992; 33:2012–2018. [PubMed: 1582806]
42. Savini G, Zanini M, Carelli V, Sadun AA, Ross-Cisneros FN, Barboni P. Correlation between retinal nerve fibre layer thickness and optic nerve head size: an optical coherence tomography study. Br J Ophthalmol. 2005; 89:489–492. [PubMed: 15774930]
43. Quigley HA, Coleman AL, Dorman-Pease ME. Larger optic nerve heads have more nerve fibers in normal monkey eyes. Arch Ophthalmol. 1991; 109:1441–1443. [PubMed: 1929937]
44. Ogden TE. Nerve fiber layer of the primate retina: thickness and glial content. Vision Res. 1983; 23:581–587. [PubMed: 6612997]
45. Hood DC, Fortune B, Arthur SN, Xing D, Salant JA, Ritch R, Liebmann JM. Blood vessel contributions to retinal nerve fiber layer thickness profiles measured with optical coherence tomography. J Glaucoma. 2008; 17:519–528. [PubMed: 18854727]
46. Chang M, Yoo C, Kim SW, Kim YY. Retinal vessel diameter, retinal nerve fiber layer thickness, and intraocular pressure in korean patients with normal-tension glaucoma. Am J Ophthalmol. 2011; 151:100–105. e1. [PubMed: 21094935]
47. Mitchell P, Leung H, Wang JJ, Rochtchina E, Lee AJ, Wong TY, Klein R. Retinal vessel diameter and open-angle glaucoma: the Blue Mountains Eye Study. Ophthalmology. 2005; 112:245–250. [PubMed: 15691558]
48. Ikram MK, de Voogd S, Wolfs RC, Hofman A, Breteler MM, Hubbard LD, de Jong PT. Retinal vessel diameters and incident open-angle glaucoma and optic disc changes: the Rotterdam study. Invest Ophthalmol Vis Sci. 2005; 46:1182–1187. [PubMed: 15790877]
49. Bennett, AG.; Rabbetts, RB. Clinical Visual Optics. London: Butterworths; 1989.
50. Bennett AG, Rudnicka AR, Edgar DF. Improvements on Littmann's method of determining the size of retinal features by fundus photography. Graefes Arch Clin Exp Ophthalmol. 1994; 232:361–367. [PubMed: 8082844]
51. Garway-Heath DF, Rudnicka AR, Lowe T, Foster PJ, Fitzke FW, Hitchings RA. Measurement of optic disc size: equivalence of methods to correct for ocular magnification. Br J Ophthalmol. 1998; 82:643–649. [PubMed: 9797665]
52. Atchison DA, Markwell EL, Kasthurirangan S, Pope JM, Smith G, Swann PG. Age-related changes in optical and biometric characteristics of emmetropic eyes. J Vis. 2008; 8:29. 1-0. [PubMed: 18484868]
53. Sardar DK, Swanland GY, Yow RM, Thomas RJ, Tsin AT. Optical properties of ocular tissues in the near infrared region. Lasers Med Sci. 2007; 22:46–52. [PubMed: 17143656]
54. Atchison DA, Smith G. Chromatic dispersions of the ocular media of human eyes. J Opt Soc Am (A). 2005; 22:29–37.

55. Vizzeri G, Bowd C, Medeiros FA, Weinreb RN, Zangwill LM. Effect of improper scan alignment on retinal nerve fiber layer thickness measurements using Stratus optical coherence tomograph. J Glaucoma. 2008; 17:341–349. [PubMed: 18703942]
56. Stewart CV, Tsai CL, Roysam B. The dual-bootstrap iterative closest point algorithm with application to retinal image registration. IEEE Trans Med Imaging. 2003; 22:1379–1394. [PubMed: 14606672]
57. Van Rijn LJ, Van der Steen J, Collewijn H. Instability of ocular torsion during fixation: cyclovergence is more stable than cycloversion. Vision Res. 1994; 34:1077–1087. [PubMed: 8160416]
58. Van Rijn LJ, Van der Steen J, Collewijn H. Eye torsion elicited by oscillating gratings: effects of orientation, wavelength and stationary contours. Vision Res. 1994; 34:533–540. [PubMed: 8303836]
59. Strouthidis NG, Yang H, Fortune B, Downs JC, Burgoyne CF. Detection of optic nerve head neural canal opening within histomorphometric and spectral domain optical coherence tomography data sets. Invest Ophthalmol Vis Sci. 2009; 50:214–223. [PubMed: 18689697]
60. Bland JM, Altman DG. Statistical methods for assessing agreement between two methods of clinical measurement. Lancet. 1986; 1:307–310. [PubMed: 2868172]
61. Lee J, Koh D, Ong CN. Statistical evaluation of agreement between two methods for measuring a quantitative variable. Comput Biol Med. 1989; 19:61–70. [PubMed: 2917462]
62. Savini G, Barboni P, Carbonelli M, Zanini M. The effect of scan diameter on retinal nerve fiber layer thickness measurement using stratus optic coherence tomography. Arch Ophthalmol. 2007; 125:901–905. [PubMed: 17620568]
63. Varma R, Skaf M, Barron E. Retinal nerve fiber layer thickness in normal human eyes. Ophthalmology. 1996; 103:2114–2119. [PubMed: 9003346]
64. Curcio CA, Allen KA. Topography of ganglion cells in human retina. J Comp Neurol. 1990; 300:5–25. [PubMed: 2229487]
65. Vizzeri G, Weinreb RN, Gonzalez-Garcia AO, Bowd C, Medeiros FA, Sample PA, Zangwill LM. Agreement between spectral-domain and time-domain OCT for measuring RNFL thickness. Br J Ophthalmol. 2009; 93:775–781. [PubMed: 19304586]
66. Gonzalez-Garcia AO, Vizzeri G, Bowd C, Medeiros FA, Zangwill LM, Weinreb RN. Reproducibility of RTVue retinal nerve fiber layer thickness and optic disc measurements and agreement with Stratus optical coherence tomography measurements. Am J Ophthalmol. 2009; 147:1067–1074. [PubMed: 19268891]
67. Hwang YH, Lee JY, Kim YY. The effect of head tilt on the measurements of retinal nerve fibre layer and macular thickness by spectral-domain optical coherence tomography. Br J Ophthalmol. 2011 [Epub ahead of print].
68. Mylonas G, Ahlers C, Malamos P, Golbaz I, Deak G, Schuetze C, Sacu S, Schmidt-Erfurth U. Comparison of retinal thickness measurements and segmentation performance of four different spectral and time domain OCT devices in neovascular age-related macular degeneration. Br J Ophthalmol. 2009; 93:1453–1460. [PubMed: 19520692]
69. Leung CK, Cheung CY, Weinreb RN, Lee G, Lin D, Pang CP, Lam DS. Comparison of macular thickness measurements between time domain and spectral domain optical coherence tomography. Invest Ophthalmol Vis Sci. 2008; 49:4893–4897. [PubMed: 18450592]
70. Knighton RW, Qian C. An optical model of the human retinal nerve fiber layer: implications of directional reflectance for variability of clinical measurements. J Glaucoma. 2000; 9:56–62. [PubMed: 10708233]
71. Scoles D, Gray DC, Hunter JJ, Wolfe R, Gee BP, Geng Y, Masella BD, Libby RT, Russell S, Williams DR, Merigan WH. In-vivo imaging of retinal nerve fiber layer vasculature: imaging histology comparison. BMC Ophthalmol. 2009; 9:9. [PubMed: 19698151]
72. Ogden TE. Nerve fiber layer of the macaque retina: retinotopic organization. Invest Ophthalmol Vis Sci. 1983; 24:85–98. [PubMed: 6826318]
73. Tan JC, Poinoosawmy D, Fitzke FW, Hitchings RA. Magnification changes in scanning laser tomography. J Glaucoma. 2004; 13:137–141. [PubMed: 15097259]

74. Sanchez-Cano A, Baraibar B, Pablo LE, Honrubia FM. Magnification characteristics of the Optical Coherence Tomograph STRATUS OCT 3000. Ophthalmic Physiol Opt. 2008; 28:21–28. [PubMed: 18201332]

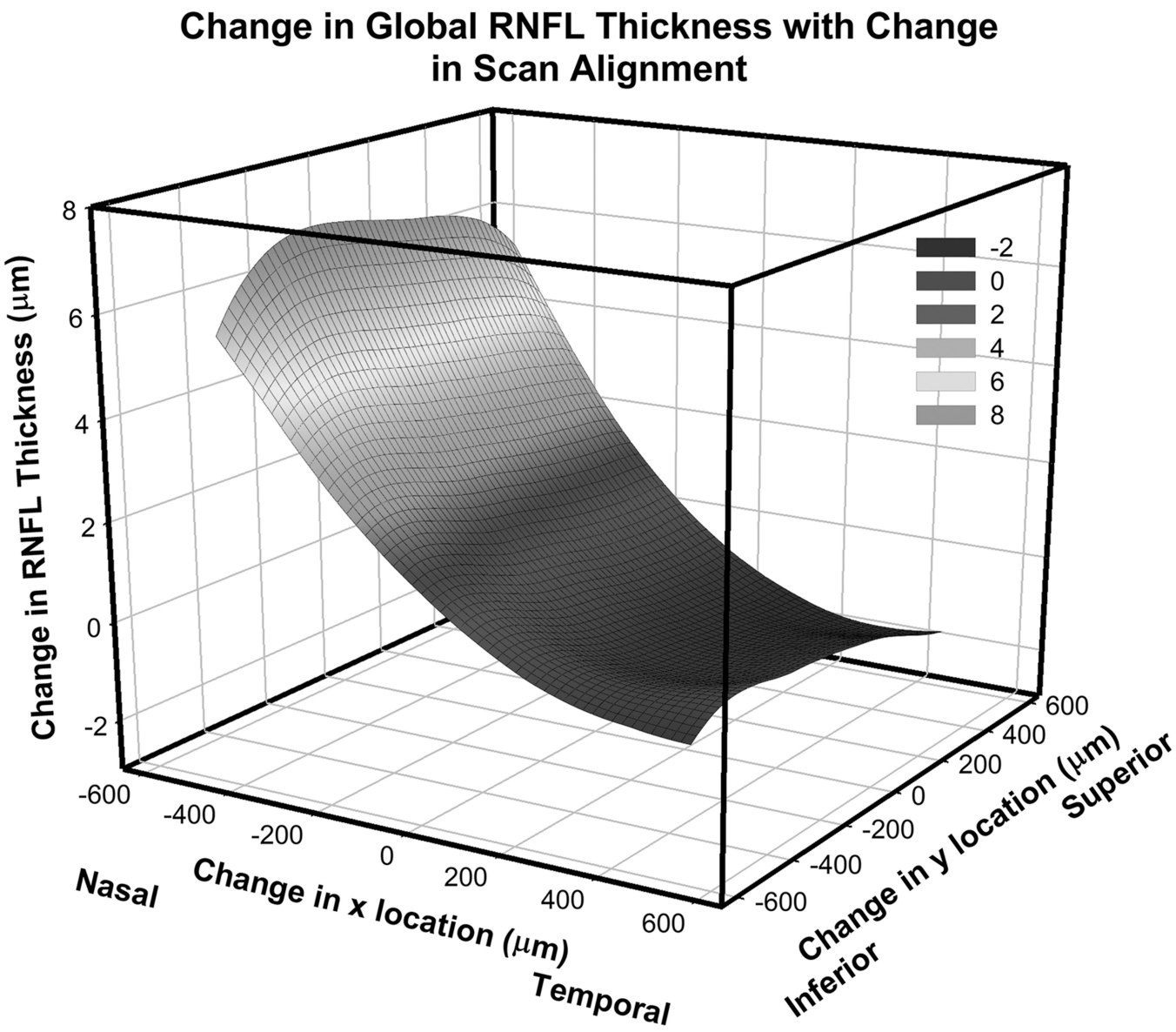

Figure 1.

The effect of scan misalignment on the measurement of RNFL thickness. The contour map represents the average change in RNFL thickness for 54 eyes, all referenced to the right eye and the center of the optic nerve. Global RNFL thickness can vary by 14.8 ± 5.3 μm within 1 mm of the center of the scan, median = 14.6 μm, range = 5.7 μm – 29.0 μm. A color version of this figure is available online at www.optvissci.com.

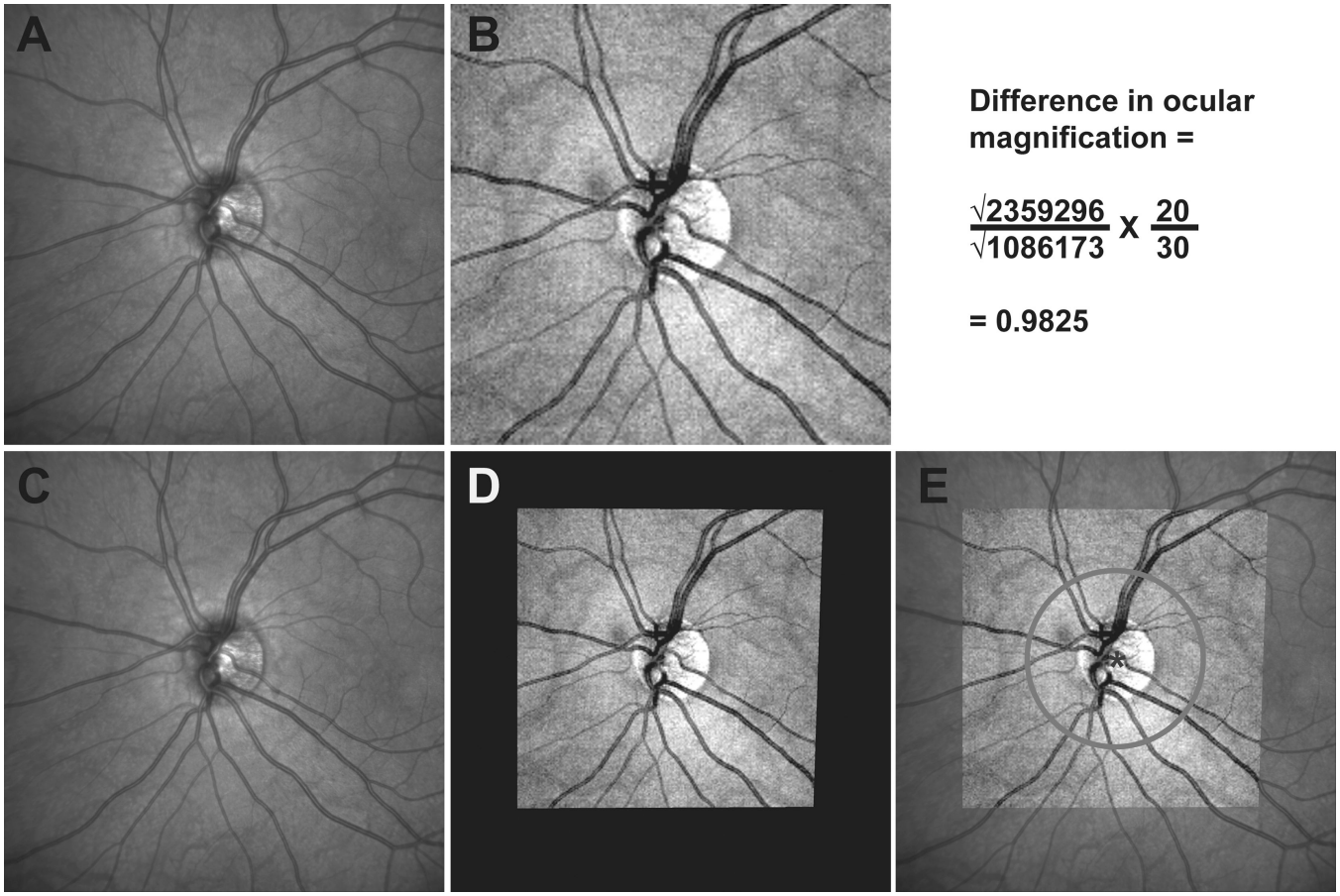

Figure 2.
The 30 degree SLO image from the Spectralis HRA+OCT(panel A) and the mean reflectance image from the Cirrus HD-OCT volume scan centered on the optic nerve (panel B) were aligned (panels C & D) and registered (panel E) to provide identical scan paths for 12 degree circular scans with each instrument. The difference calculation for ocular magnification for this data set is illustrated above figure E. A color version of this figure is available online at www.optvissci.com.

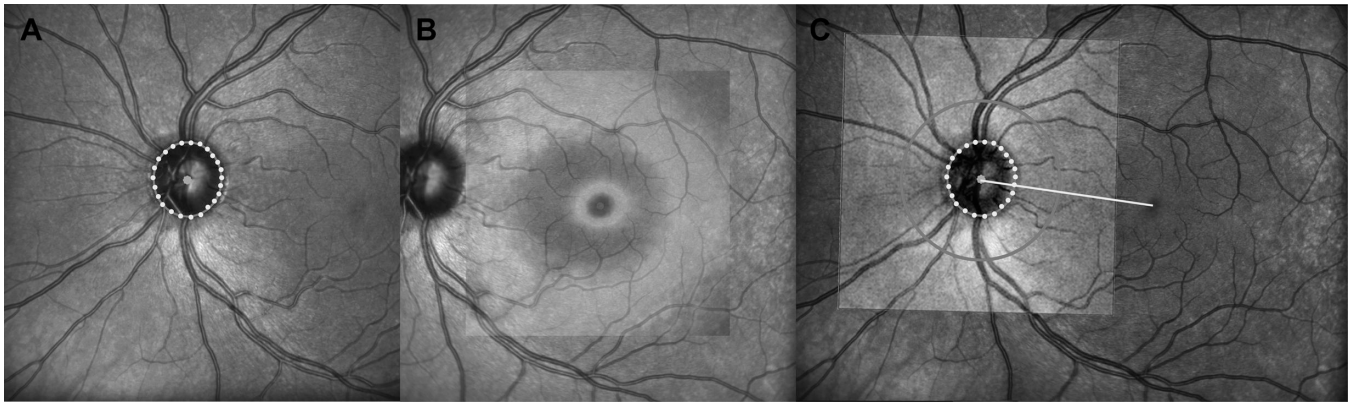

Figure 3.

Procedures to correct the SD-OCT images for torsional eye movements by identifying a reference line connecting the center of the ONH to the center of the fovea pit. A. First locations of the opening of the neural canal (NCO) were identified on 12 radial B-scans through the optic nerve and were transferred onto the infrared scanning laser ophthalmoscope (SLO) image, and fit with an ellipse. B. Second, the center of the fovea pit was identified in the retina thickness map as the region with the thinnest retina (darkest blue color) and geometric center of the pit was identified from the geometric center of a series of iso-thickness circles best fit to the pit thickness at varying heights. C. An example of the registered foveal and optic nerve SLO images illustrating the line through the NCO and foveal pit center that was used as reference for torsional alignment of the retinal images. A color version of this figure is available online at www.optvissci.com.

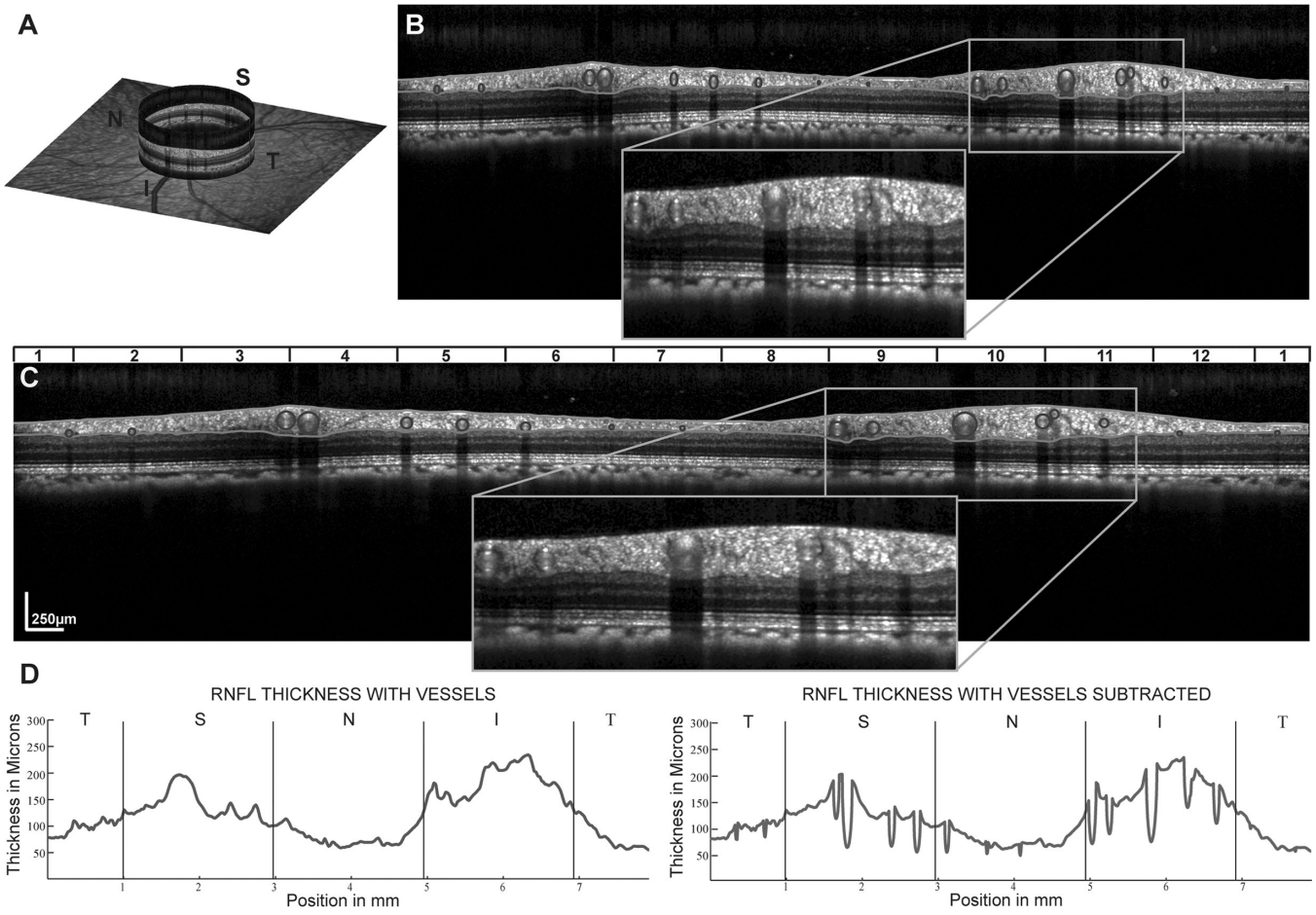

Figure 4.

The identification and removal of the major vasculature from the RNFL. A. An example of the RNFL B-scan image illustrating the locations of vessels. B&C Shadows in RNFL B-scans identify major retinal vessels in B-scan images of Spectralis scans in the unscaled image (B) and after rescaling the B-scans to 1:1 μm (C) where the retinal vessels can be identified as circular structures within the scan. D. RNFL thickness plots demonstrating the effect of removing the vessel contribution to RNFL thickness. It should be noted that only portions of the vessel within the RNFL segmentation were subtracted to create the thickness plot and in subsequent calculations of RNFL and area measures. A color version of this figure is available online at www.optvissci.com.

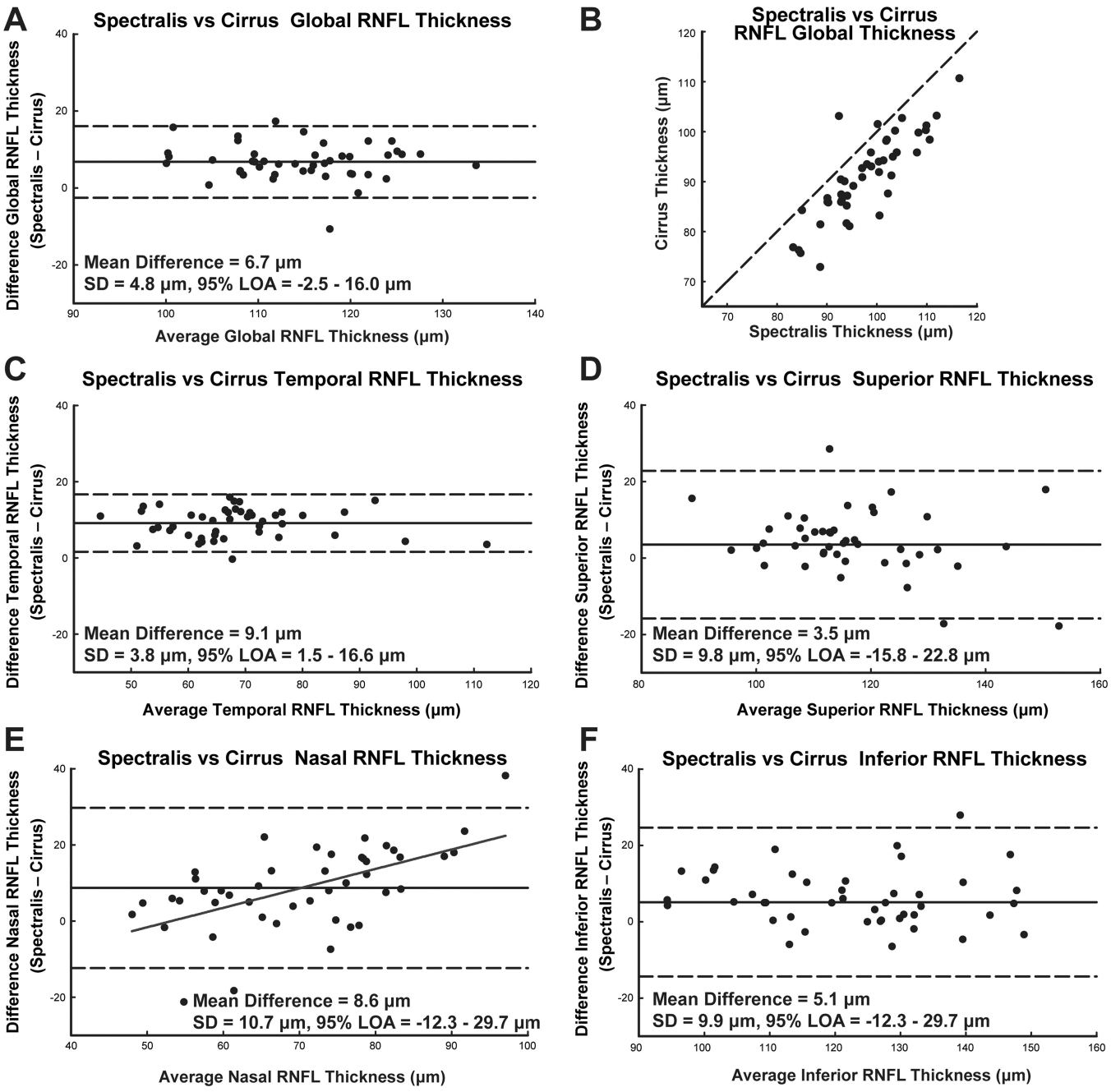

Figure 5.

The limits of agreement between RNFL thickness by Spectralis and Cirrus SD-OCT instruments, using the manufacturer's thickness algorithms. A. The Bland-Altman plot for the agreement between global thickness measurements. B. Thickness measures from the two instruments and their deviation from the 1:1 line. C-E. Bland-Altman plots to illustrate the limits of agreement for each quadrant, demonstrating that the relationship between the thickness difference and average thickness is not statistically significant, except the nasal quadrant (E, slope = 0.51, intercept = −27.19, $R^2 = 0.34$, $p < 0.01$).

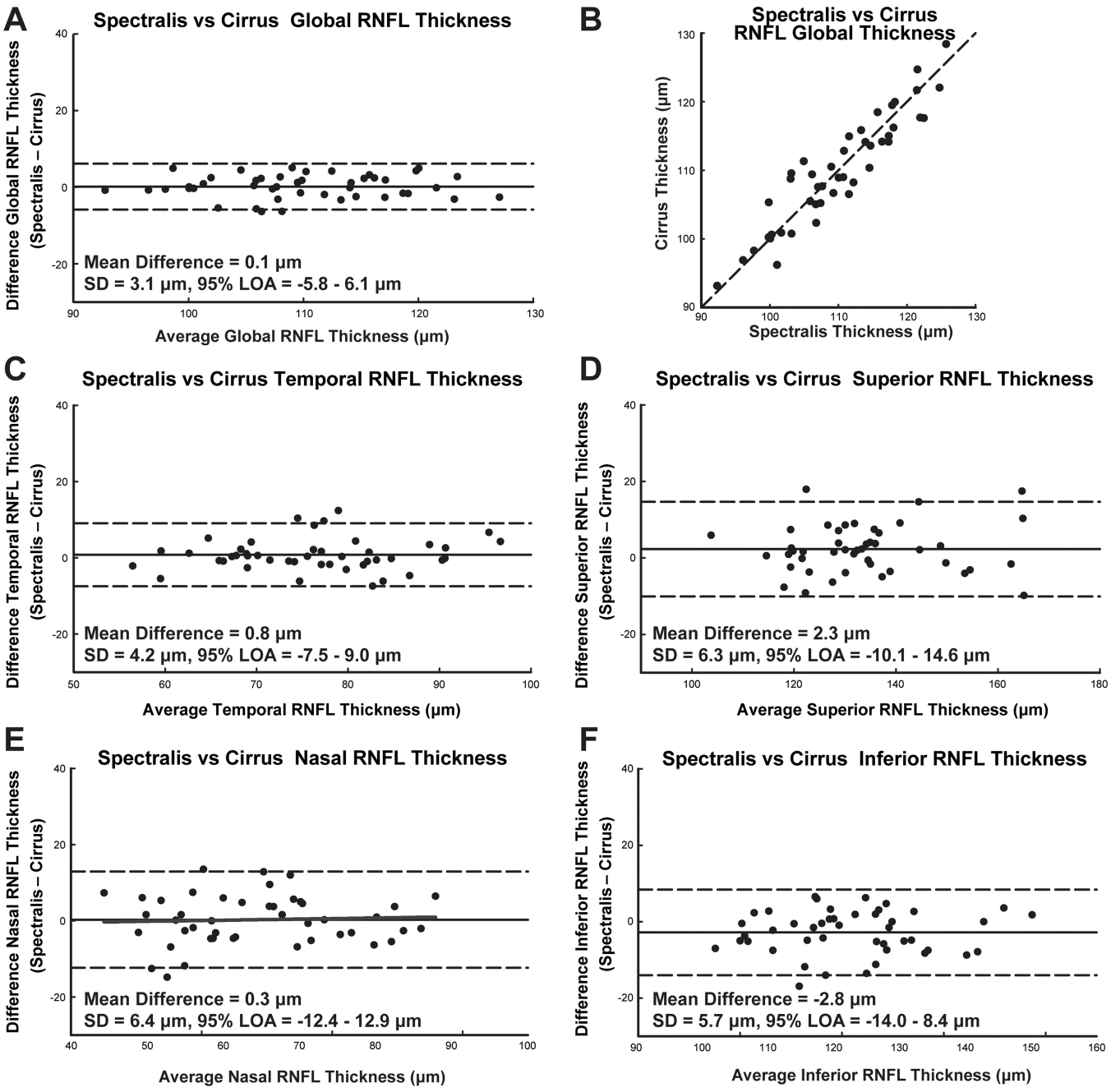

Figure 6.

The limits of agreement between RNFL thickness by Spectralis and Cirrus SD-OCT instruments, using custom algorithms for scaling, rotation, registration, and segmentation, but without vessel compensation. Other details are as Fig. 5. The Bland-Altman analysis for RNFL thickness via custom image analysis demonstrates well correlated measurements and high ICCs for all quadrants with no statistical relationship between the thickness difference and average thickness. E. For the nasal quadrant, the difference in thickness measures between instruments did not have a systematic trend (slope = 0.02, intercept = −1.9, $R^2 <$ 0.01, p = 0.75).

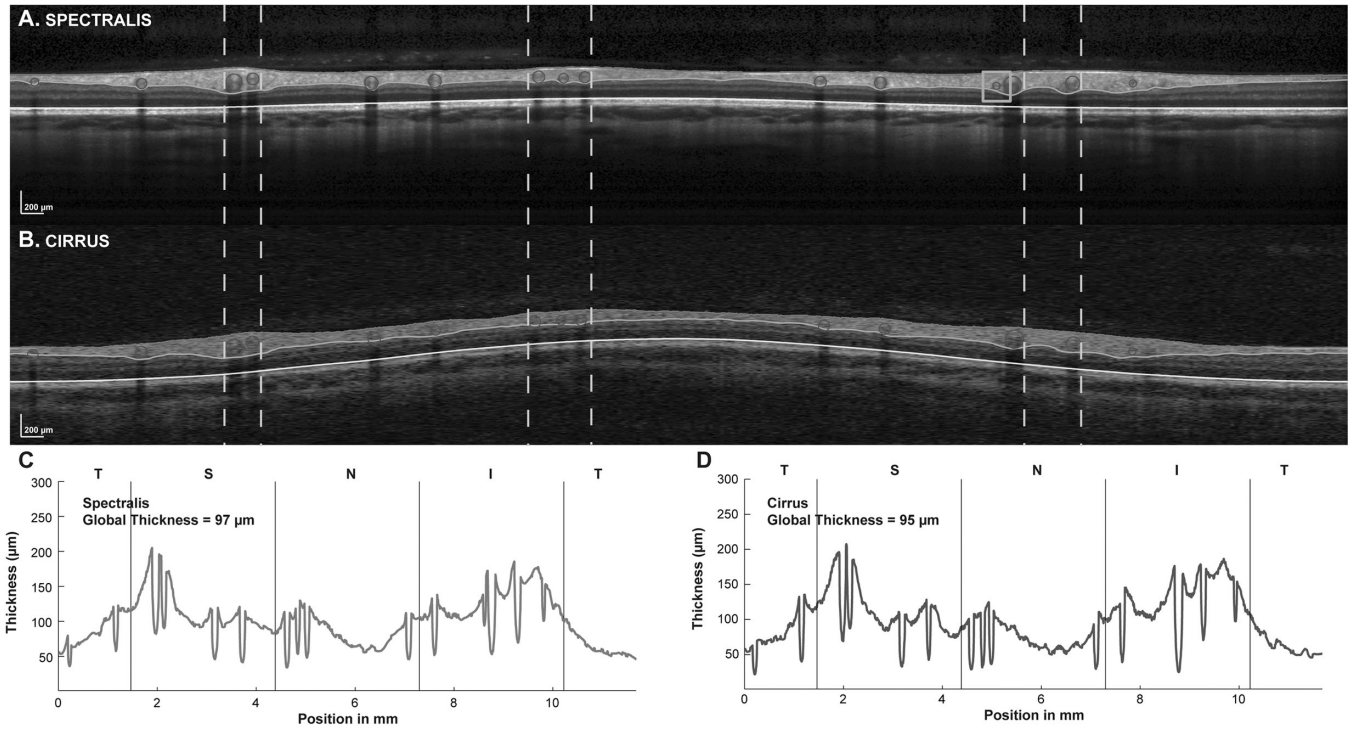

Figure 7.

Examples of TSNIT functions for Spectralis and Cirrus SD-OCT after incorporating vessel identification and compensation in the B-scans, and with identical scan paths from the two instruments. The B-scans for the Spectralis (A) and Cirrus (B) are presented with white vertical dashed lines illustrating the location of some of the major retinal vessels in the two images. Although the vessels localized well, there were some small misalignments. Overall, a similar number of vessels were identified in both B-scans, but with some smaller vessels being missing in one or the other B-scans occasionally, as illustrated by the orange box in A. The TSNIT plots for both Spectralis (C) and Cirrus (D) instruments show dips at similar locations and nearly equal global thicknesses after compensation for the major retinal vasculature. A color version of this figure is available online at www.optvissci.com.

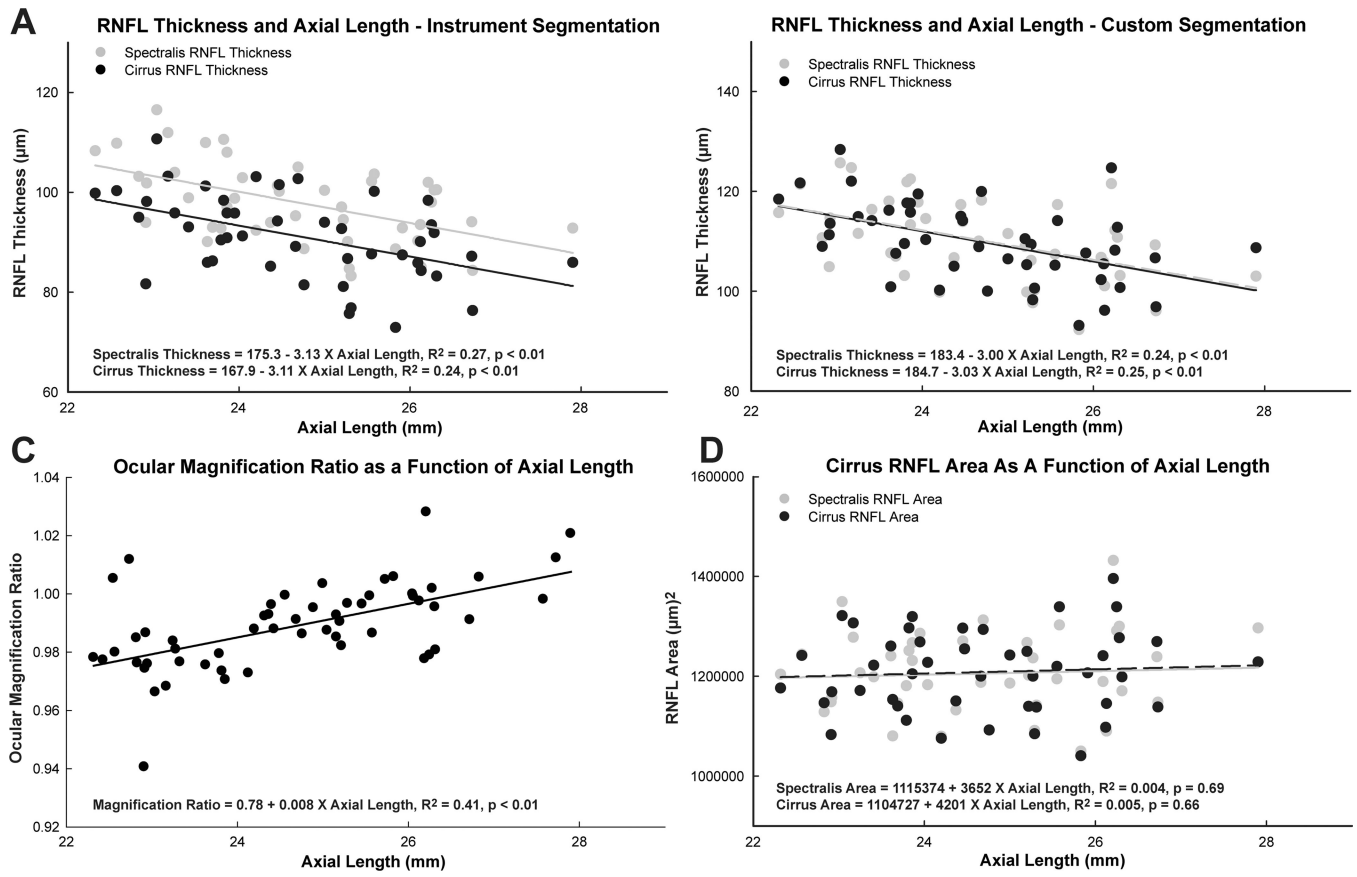

Figure 8.

Relationships between RNFL measurement parameters and axial length using Spectralis and Cirrus SD-OCT instruments. A. The relationship between RNFL thickness and axial length was significant for both instruments, with similar slopes for linear regression, but with an approximately constant difference between instruments across the range of axial lengths. B. With custom segmentation, the relationship between thickness and axial length was not significantly different for the two instruments. C. The relationships between the ocular magnification ratio and axial length were significantly different between the two instruments. D. The differences in ocular magnification did not have a significant influence on the RNFL area computations and the RNFL area was not statistically related to axial length.

Table 1

Instrument algorithm RNFL thickness measures for quadrant and clock hours for Cirrus and Spectralis SD-OCT. Along with the paired t-test statistic, the intraclass correlation coefficient (ICC) with 95% confidence intervals provides a measure of agreement for the two segmentation algorithms.

	Cirrus		Spectralis			95% Confidence		Paired t-test
	Mean (μm)	Std Dev	Mean (μm)	Std Dev	ICC	Lower	Upper	
Global	91.17	8.42	97.92	7.94	0.623	−0.074	0.864	<0.001
Temporal	63.71	12.96	72.79	12.71	0.765	−0.054	0.938	<0.001
Superior	115.03	14.94	118.52	12.98	0.734	0.552	0.847	0.022
Nasal	65.89	10.06	74.56	15.88	0.559	0.119	0.780	<0.001
Inferior	120.08	16.39	125.21	15.21	0.764	0.544	0.876	0.001
Sector 1	49.57	8.70	58.81	10.87	0.631	−0.071	0.887	<0.001
Sector 2	77.15	19.18	85.73	17.53	0.853	0.068	0.957	<0.001
Sector 3	125.78	21.95	134.40	23.92	0.780	0.491	0.895	<0.001
Sector 4	114.12	24.88	112.97	22.18	0.797	0.658	0.883	0.613
Sector 5	105.17	16.77	108.18	18.31	0.794	0.653	0.882	0.075
Sector 6	80.23	17.45	90.59	23.26	0.743	0.256	0.893	<0.001
Sector 7	55.31	9.79	62.95	15.50	0.414	0.110	0.640	<0.001
Sector 8	62.12	10.60	70.13	16.12	0.571	0.182	0.776	<0.001
Sector 9	95.75	18.21	99.21	18.00	0.701	0.517	0.824	0.100
Sector 10	134.94	26.79	137.62	27.59	0.801	0.666	0.885	0.301
Sector 11	129.53	26.72	138.45	25.62	0.885	0.465	0.959	<0.001
Sector 12	64.40	15.79	73.37	15.84	0.759	0.080	0.915	<0.001

Table 2

Average thickness and paired t-test and ICC for scans centered to match that of Spectralis 12 degree circular scans.

	Cirrus				Cross Correlated	Paired t-test
	Global Thickness	Std Dev	ICC	Paired t-test		
Global	90.83	8.42	0.645	<0.001	0.645	<0.001
Temporal	62.95	11.85	0.721	<0.001	0.837	<0.001
Superior	111.59	13.71	0.794	<0.001	0.886	<0.001
Nasal	66.85	11.03	0.574	<0.001	0.649	<0.001
Inferior	124.26	16.64	0.904	0.054	0.905	0.056

Table 3

Instrument algorithm vs. Custom RNFL thickness measures for quadrant and clock hours for Cirrus and Spectralis SD-OCT.

	Cirrus				Spectralis			
	Instrument Global Thickness (μm)	Custom Global Thickness (μm)	ICC	Paired t-test	Instrument Global Thickness (μm)	Custom Global Thickness (μm)	ICC	Paired t-test
Global	91 ± 8	110 ± 8	0.227	<0.001	98 ± 8	110 ± 8	0.405	<0.001
Temporal	64 ± 13	76 ± 10	0.515	<0.001	73 ± 13	77 ± 10	0.803	<0.001
Superior	115 ± 15	133 ± 14	0.407	<0.001	119 ± 13	135 ± 15	0.463	<0.001
Nasal	66 ± 10	88 ± 13	0.249	<0.001	75 ± 16	89 ± 14	0.539	<0.001
Inferior	120 ± 16	143 ± 15	0.361	<0.001	125 ± 15	140 ± 15	0.600	<0.001
Sector 1	50 ± 9	59 ± 6	0.303	<0.001	59 ± 11	60 ± 6	0.542	0.520
Sector 2	77 ± 19	83 ± 13	0.588	0.005	86 ± 18	84 ± 12	0.692	0.231
Sector 3	126 ± 22	138 ± 27	0.636	<0.001	134 ± 24	138 ± 29	0.768	0.233
Sector 4	114 ± 25	140 ± 24	0.405	<0.001	113 ± 22	144 ± 21	0.404	<0.001
Sector 5	105 ± 17	119 ± 22	0.540	<0.001	108 ± 18	123 ± 23	0.594	<0.001
Sector 6	80 ± 17	110 ± 24	0.334	<0.001	91 ± 23	112 ± 24	0.570	<0.001
Sector 7	55 ± 10	78 ± 16	0.204	<0.001	63 ± 15	77 ± 15	0.486	<0.001
Sector 8	62 ± 11	77 ± 11	0.304	<0.001	70 ± 16	76 ± 12	0.593	0.001
Sector 9	96 ± 18	111 ± 16	0.469	<0.001	99 ± 18	111 ± 17	0.684	<0.001
Sector 10	135 ± 27	152 ± 25	0.603	<0.001	138 ± 28	147 ± 25	0.836	<0.001
Sector 11	130 ± 27	166 ± 23	0.375	<0.001	138 ± 26	162 ± 21	0.525	<0.001
Sector 12	64 ± 16	84 ± 15	0.420	<0.001	73 ± 16	86 ± 16	0.600	<0.001

Table 4

Major retinal vascular contribution to RNFL thickness. Vascular contribution to the RNFL is similar for the two instruments as illustrated by the paired t-test statistic.

	Spectralis			Cirrus			Paired t-test (p),vascular contribution
	Thickness with vessels (μm)	Thickness Without Vessels (μm)	% Vascular contribution	Thickness with vessels (μm)	Thickness without Vessels (μm)	% Vascular contribution	
Global	110 ± 8	97 ± 7	11.8 ± 1.5	110 ± 8	97 ± 7	11.3 ± 1.6	0.076
Temporal	77 ± 10	74 ± 9	4.0 ± 2.5	76 ± 10	73 ± 9	3.8 ± 2.9	0.617
Superior	135 ± 15	116 ± 12	14.3 ± 3.0	133 ± 14	115 ± 13	13.4 ± 2.9	0.054
Nasal	89 ± 14	80 ± 11	10.0 ± 3.4	88 ± 13	80 ± 11	9.7 ± 3.5	0.558
Inferior	140 ± 15	120 ± 14	14.6 ± 2.6	143 ± 15	123 ± 14	14.2 ± 2.4	0.223

Table 5

Custom algorithm RNFL thickness measures for quadrant and clock hours for Cirrus and Spectralis SD-OCT. Along with the paired t-test statistic, the intraclass correlation coefficient (ICC) with 95% confidence intervals provides a measure of agreement for the two segmentation algorithms. Thickness measures are before compensation for major retinal vasculature.

	Cirrus		Spectralis			95% Confidence		Paired t-test (p)
	Mean (μm)	Std Dev	Mean (μm)	Std Dev	ICC	Lower	Upper	
Global	109.90	8.03	110.16	8.07	0.921	0.861	0.956	0.591
Temporal	75.82	9.58	76.72	10.01	0.902	0.823	0.945	0.165
Superior	132.64	14.34	135.03	14.52	0.893	0.801	0.942	0.015
Nasal	88.33	13.36	88.72	13.60	0.884	0.799	0.935	0.689
Inferior	143.16	14.78	140.49	15.10	0.910	0.816	0.953	0.004
Sector 1	58.96	5.76	59.61	5.54	0.774	0.625	0.869	0.258
Sector 2	83.39	12.66	83.58	12.35	0.885	0.799	0.935	0.835
Sector 3	138.24	27.97	137.62	28.56	0.944	0.901	0.969	0.665
Sector 4	140.44	23.79	144.12	21.01	0.853	0.742	0.917	0.042
Sector 5	119.24	21.79	123.37	23.00	0.902	0.802	0.949	0.004
Sector 6	109.55	23.97	112.48	23.77	0.861	0.760	0.921	0.121
Sector 7	78.45	15.88	77.15	14.88	0.858	0.757	0.919	0.293
Sector 8	77.00	11.34	76.55	11.55	0.647	0.438	0.790	0.756
Sector 9	111.67	15.75	111.44	17.35	0.831	0.712	0.904	0.874
Sector 10	151.78	25.38	147.28	24.67	0.942	0.842	0.974	<0.001
Sector 11	165.70	22.60	162.48	21.41	0.897	0.813	0.943	0.030
Sector 12	84.37	14.61	86.24	15.61	0.903	0.828	0.946	0.060